J Mol Model (2013) 19:3671–3682
DOI 10.1007/s00894-013-1904-y

ORIGINAL PAPER

Natural velvet antler polypeptide conformation prediction and molecular docking study with TGF-β1 complex

Yu-Dong Shang · Ji-Long Zhang · Qing-Chuan Zheng

Received: 9 November 2012 / Accepted: 28 May 2013 / Published online: 15 June 2013

Abstract Based on the chain A structures of hemoglobin (PDB code: 1HDS, 1IBE, 1FAW, 3AT5), the three dimensional (3D) structure of natural velvet antler polypeptide (nVAP) was constructed by homology modeling and molecular dynamics (MD) method. The structural rationality was further checked by Profile-3D and Procheck, both of which confirmed that the 3D structure of nVAP was reasonable. The modeled structure indicates that the stable conformation of nVAP is composed of two α-helixes. The extracellular domains of transforming growth factor-β1 receptor I (TβRI-ED) and II (TβRII-ED) were docked with nVAP, respectively. The results show that both of TβR-EDs have high affinity with nVAP which locates near the active center of TβRII-ED integrating with transforming growth factor-β1 (TGF-β1). Otherwise, nVAP can also insert near the "pre-helix extension" of TβRI-ED, which is the key domain to interact on TGF-β1 and TβRII-ED. With the perturbation of nVAP, TβRI-ED can not be recruited by TGF-β1:TβRII-ED complex rigorously. The intracellular domain of TβRI (TβRI-ID) is not phosphorylated and activated by TβRII. This study shows that nVAP prefers tethering TβRI-ED which is more crucial in TGF-β1:TβRII-ED:TβRI-ED complex. Thus nVAP can disturb the TGF-β1 binding pattern by interacting on TβRs (TβRI and TβRII), further intercepting TGF-β1 pathway downstream.

Keywords Docking · Hepatic fibrosis · Molecular dynamics · Natural velvet antler polypeptide · Transforming growth factor-β1

Y.-D. Shang · J.-L. Zhang · Q.-C. Zheng (✉)
State Key Laboratory of Theoretical and Computational Chemistry, Institute of Theoretical Chemistry, Jilin University, Changchun 130023, Jilin, People's Republic of China
e-mail: zhengqc@jlu.edu.cn

Introduction

Velvet antler is a kind of valuable Chinese crude drug, which has extensive pharmacological activities and function for medical care. The content of protein and polypeptide is above 50 %. Guan [1] extracted a monomer velvet antler polypeptide with 32 amino acid residues from the total velvet antler polypeptide (tVAP) by means of chromatography. The protein content which is determined by mass spectrometry was high up to 98.7 % and the molecular mass was 3263.4 Da. The novel polypeptide is named natural velvet antler polypeptide (nVAP) with characters of white, silkiness, diffluent and viscousness. The residue Met32 in C terminal is oxidated. The 3D structure is significant to reveal the mechanism of receptor-ligand interaction and the biochemical process, but the 3D structure of nVAP has not been reported until now.

In physiological state, transforming growth factor (TGF)-β1, -β2, and -β3 are 25 kDa polypeptides that play crucial nonoverlapping roles in embryogenesis, cell growth, differentiation, development, carcinogenesis and immune response [2–4]. TGF-β1 is considered to be one of the strongest factors promoting hepatic fibrosis during the course of priming, progressing and forming of hepatic cirrhosis [5]. The TGF-β signaling pathway is initiated through the binding of mature TGF-β to transmembrane transform growth factor-β1 receptor II (TβRII), followed by the recruitment of TβRI and subsequently the activation of TβRI by TβRII. Intracellularly, the activated TβRI phosphorylates the major downstream signaling molecules Smad2 and Smad3 proteins, which then form a complex with Smad4. This complex translocates into nucleus and regulates the transcription of specific genes [6, 7] (Fig. 1). The extracellular matrix (ECM) which causes pathological hepatic fibrosis is therefore generated and secreted.

A small molecule, an antibody effector and a peptide that bind to key signaling components serve as valuable probes. TβRI is a key molecule within the TGF-β signaling pathway.

TGFβ1:TβRII:TβRI+Smad2/3 $\xrightarrow{\text{phosphorylate}}$ phospho-Smad2/3+Smad4

$\xrightarrow{\text{intranuclear}}$ Smad2/3/4 $\xrightarrow{\text{DNA binding partner}}$ Gene regulation

Fig. 1 TGF-β signaling pathway. TβRII which forms non-covalent homodimers, binds to the covalently linked TGF-β homodimer. The TGF-β:TβRII complex then recruits two copies of TβRI. This quinary complex enables the active TβRII to catalyze the phosphorylation domain of TβRI. The adjacent kinase domain catalyzes the phosphorylation and activation of receptor-regulated Smad2 and Smad3. Phosphorylated Smad2 and Smad3 bind to Smad4, and the complex translocates into the nucleus. Once in the nucleus, the Smads bind to different DNA binding partners to control gene expression

Therefore, it has been believed as a critical target for the blockage of TGF-β signaling [8, 9]. Functional inhibition of TβR-I has been shown to be able to suppress the fibrosis and cancer in animal models [10–12]. In TGF-β1 complex, the function of TβRII is to bind TGF-β1 correctly and trans-phosphorylated by TβRI with low affinity [13, 14]. Specifically, both of the receptors have a common pattern of disulfide bonds, stabilizing a structure feature named the "three-finger toxin fold" [15]. The detailed molecular mechanism involves ligand-induced receptor activation. The determination of the binding mechanism and the related thermodynamic and kinetic parameters are of prime importance [16].

In TGF-β1 signaling pathway, nVAP plays a part in the course of extracellular domain. As an exogenous material, nVAP can bind to both TβRI-ED and TβRII-ED, weakening the interaction between TGF-β1 and TβRs. Further, the secretion of ECM is degraded and hepatic fibrosis thus would be reversed. Comparing with the research progress of small molecule inhibitor of TGF-β1, there are only a few studies on the peptide inhibitor of TGF-β1 complex. The 3D structure of nVAP was predicted by homology modeling, and then we exploited the kinetic behavior of nVAP and TGF-β1 complex. Then molecular docking studies were performed between nVAP and TGF-β1 subunits based on serial experiments, pursuing the possible binding site of nVAP with TβRII-ED and TβRI-ED. Our investigation revealed the

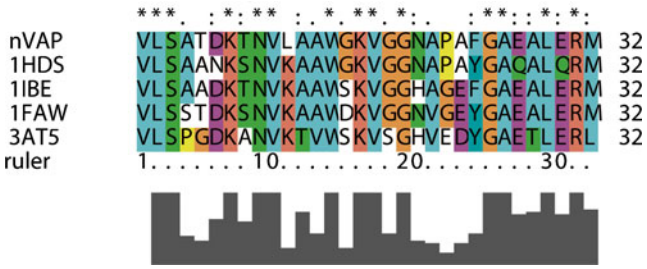

Fig. 2 Sequence alignment of nVAP and templates. The amino acid sequence was taken as probe. In nVAP sequence, there are residues of similar character with template sequence marked ":". Residues have less similarity marked ".". Residues have no similarity marked a "blank". Other residues match very well (marked "*"). The *dark gray* strip marks matching extent between the residue of nVAP and corresponding residue of template

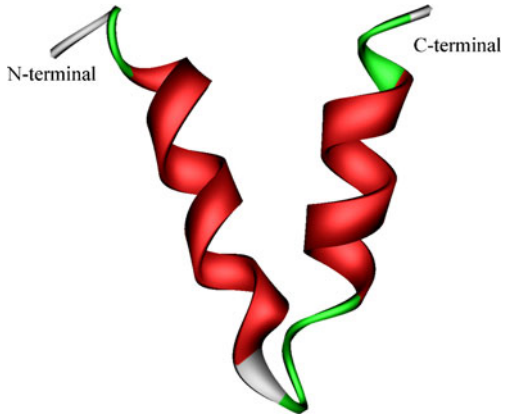

Fig. 3 3D-structure of nVAP. In the docked structure, the α-helix is represented by *red* color. The β-turn is represented by *green* color. The loop is represented by *white* color

inhibitive mechanism of nVAP on TGF-β1 signaling pathway. The results provide theoretical support for reversing hepatic fibrosis.

Theoretical methods

Homology modeling

To find related proteins as the templates for homology modeling, BLAST search algorithm [17] was used for the search online (http://www.ncbi.nih.gov/). The obtained sequences were imported into the ClustalX program (version 1.83). Then, the Modeler module in Discovery Studio software package (version 2.5) [18] was performed to construct the initial 3D structure of nVAP. During the process, we built

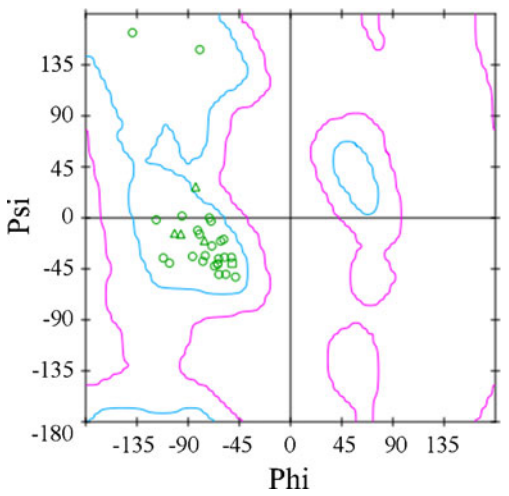

Fig. 4 The Ramachandran plot of nVAP. The *green dots* represent residues of nVAP. The dots surrounded by *cyan curve* indicate the residues are in the most favored region. The only dot outside the cyan region but in the *pink region* means the residue is in additional allowed region

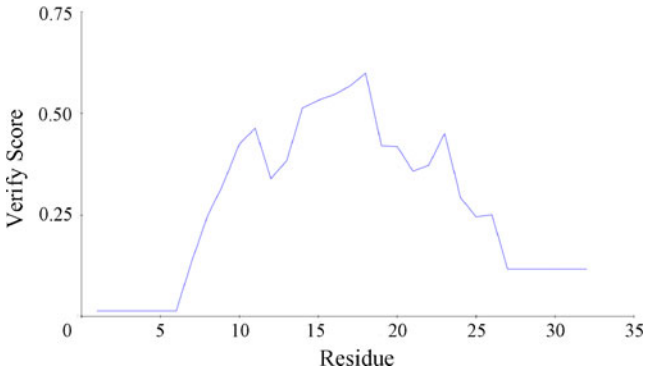

Fig. 5 The evaluation of the nVAP final structure by Profile-3D program. All the scores of residues are above zero. It means the residues are in credible positions

five homology models and adopted a high level in the optimization of nVAP including the side chains. The side chain isomerism, such as oxidizing sulphur atom of Met32, was developed after homology modeling. The loop region of nVAP was also refined. Through the procedure mentioned above, an initial model was thus completed.

Molecular dynamics simulation and refinement of nVAP structure

All the MD simulations were performed on Inspur workstations using the Amber10 [19] software package. The ff03 force field [20] was used for energy minimization and MD simulations. The charge of nVAP model was neutralized by xleap module of Amber10. An explicit solvent model TIP3P water box [21] was used with the distance of 10 Å between nVAP surface and water box boundary. Before the MD simulations, a series of energy minimization (EM) was performed. With restraint on nVAP, a minimization of 1000-step steepest descent (SD) and 1000-step conjugate gradient (CG) were carried out. The constraint force constant on peptide bond was 500 $kcal \cdot mol^{-1} \cdot Å^{-2}$. After that, without any restraint on the whole system, a minimization of 3000-step SD and 4000-step CG was carried out. A heating simulation was performed steps from 0 to 300 K in 500 ps. A weak constraint force constant value of 10 $kcal \cdot mol^{-1} \cdot Å^{-2}$ was used for nVAP. After heating, a NPT ensemble of 1 atm and 300 K was applied for an 8 ns equilibrium simulation without any

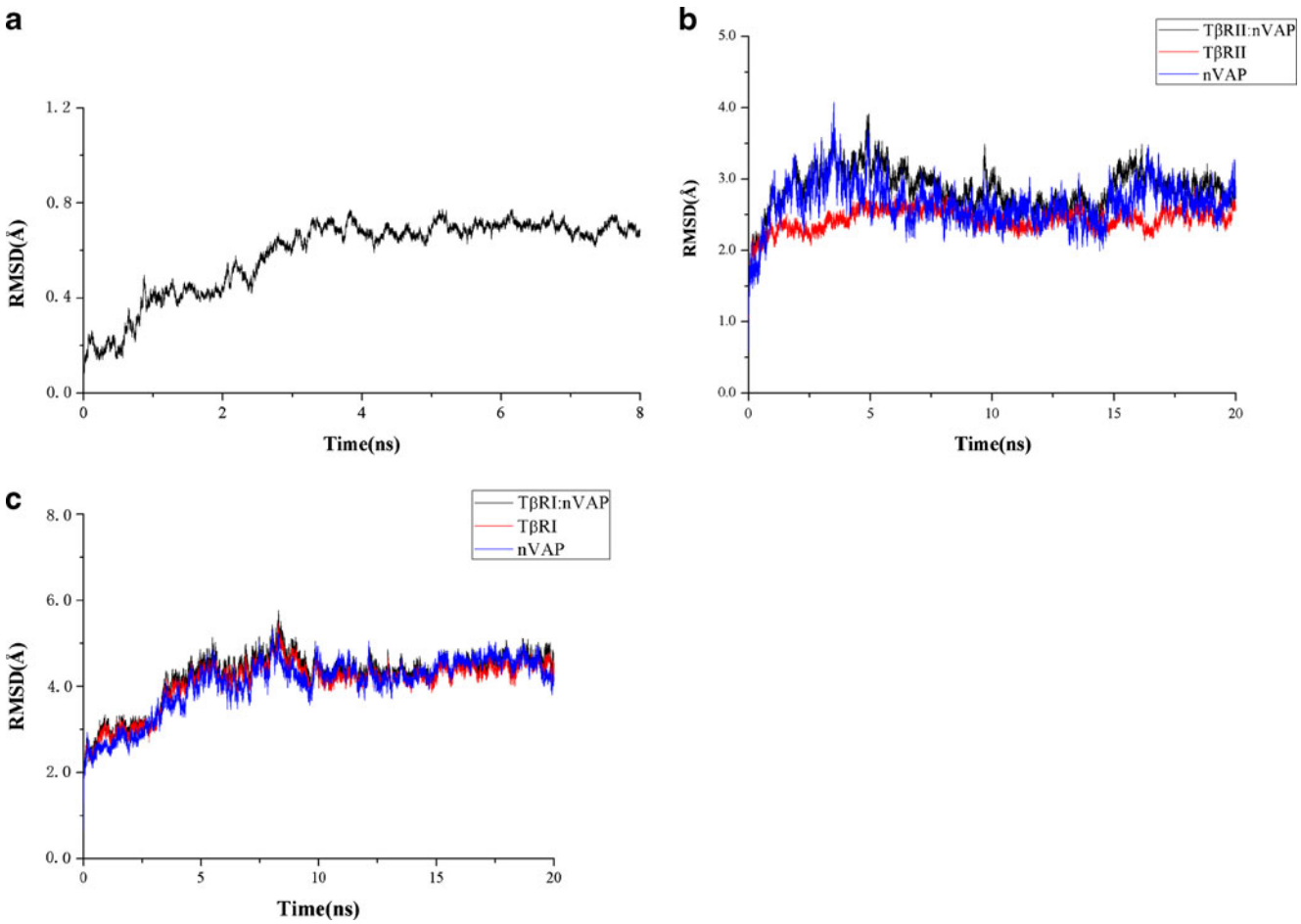

Fig. 6 **a** The RMSD plot of nVAP within 8 ns simulation. **b** The RMSD plots of TβRII-ED:nVAP complex, subunits of TβRI-ED and nVAP within 20 ns MD simulation. **c** The RMSD plots of TβRI-ED:nVAP complex, subunits of TβRI-ED and nVAP within 20 ns MD simulation figure captions

constraint. Periodic boundary conditions were applied to the system to obtain consistent behavior. The cutoff value of nonbonded interaction was set to 12 Å. The particle mesh Ewald (PME) method was employed for the computation of long-range electrostatic forces. The integral step length was 1.0 fs. All the bonds containing hydrogen were not restrained. A simple Leapfrog integrator was used to propagate the dynamics, with the collision frequency of 1 ps^{-1}. A Langevin thermostat was adopted. The relaxation time for barostat bath was 2.0 ps.

After the MD simulation optimization procedure, the structure was checked using Profile-3D [22] and Procheck [23]. The Profile-3D method measures the compatibility of amino acid sequence with a known 3D protein structure. Procheck examines the reliability of the backbone torsion angles (Φ-Ψ) of the target peptide.

Docking study

The structural information from the theoretically modeled complex may help us to clarify the relationship between structure and function. The initial structures of TGF-β1 and TβRII-ED were taken from Protein Data Bank (PDB code: 3KFD chain A and E). The structure of TβRI-ED was taken from 2PJY chain C. ZDOCK module [24] of Discovery Studio 2.5 was used to perform all the protein docking simulations. The CHARMm Polar H force field [25] was applied to depict all the atoms except non-polar H in docking. We set the angular step size to be 15 and adopted 10 Å distance cutoff in docking process; 2000 top poses were generated and then classified into 60 clusters. The cutoff value of RMSD was 6.0 Å and interface cutoff was 9.0 Å. Zrank scoring algorithm was then tested on ZDOCK benchmark dataset version 2.5 [24]. There were four steps for us to perform docking process: First, we docked TGF-β1 and TβRII-ED to evaluate the reliability of ZDOCK comparing with crystal structure 3KFD; Second, we built the nVAP:TβRII-ED:TGF-β1 complex. The order was that nVAP was docked with TβRII-ED, then TGF-β1 was docked to the aforesaid complex; Third, we constructed TβRI-ED:TβRII-ED:TGF-β1 complex. That is, TβRI-ED was docked with TβRII-ED:TGF-β1 complex; Finally, we established nVAP:TβRI-ED:TβRII-ED:TGF-β1 complex. The order was as follows: nVAP was docked to TβRI-ED, then the binary complex was docked with the TβRII-ED:TGF-β1 complex. Till now, the docking jobs were completed. We designed two cases for the docking of nVAP to the TβRI-ED:TβRII-ED:TGF-β1 ternary complexes: 1. nVAP was docked with TβRII-ED. After that, nVAP:TβRII-ED complex was docked with TGF-β1, but without TβRI-ED. The step aimed to evaluate the effect of nVAP on the binding of TGF-β1 to TβRII-ED; 2. At first, nVAP was docked with TβRI-ED to obtain nVAP:TβRI-ED complex. Then, the binary complex was docked with the TβRII-ED:TGF-β1 complex, resulting in the nVAP:TβRI-ED:TβRII-ED:TGF-β1 quaternary complex. The effect of nVAP on the binding of TβRI-ED to TβRII-ED:TGF-β1 complex could be accessed by the comparison of the quaternary complex with the TβRI-ED:TβRII-ED:TGF-β1 complex. The docking and MD results were visualized and analyzed through Discovery Studio 2.5 Visualizer [18]. The calculation for the interaction energy between ligand and receptor was performed by the "Calculate Interaction Energy" [18, 25, 26] module in Discovery Studio 2.5 program, including van der Waals energy, electrostatic energy and total energy. In the calculation, each subunit in complex was defined as a "group" to determine the interaction of consecutive residues. For the MD results, the interaction energies were calculated by the average structure of multiple conformations in the equilibrated trajectories. The nonbond list radius was 14 Å. Within this cutoff distance, nonbonded interactions between atom pairs were scaled smoothly using a switching function from 10 to 12 Å. "Anchoring energy" was used to describe the interaction energy among the interfacial residues in complexes, which contribute to fix the interactional subunits in proper locations. When the energy value increases, it indicates that the interaction among residues is weakened. On the contrary, it means that the interaction is strengthened.

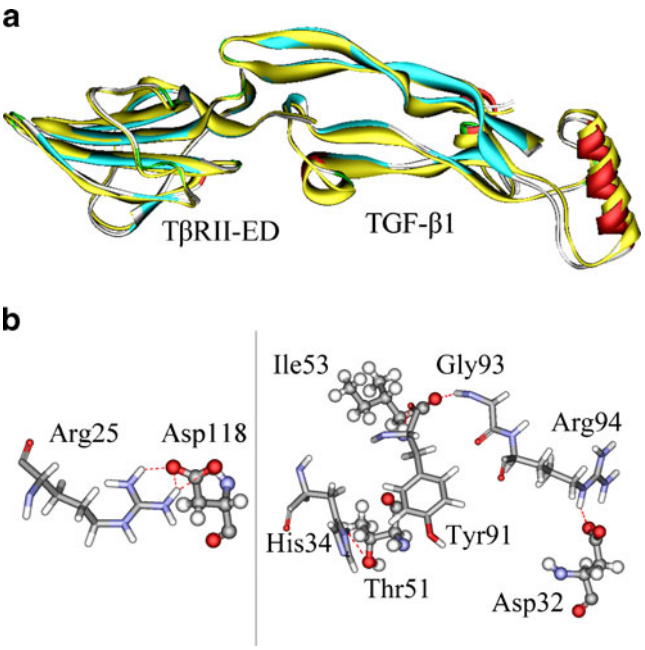

Fig. 7 Docking result of TGF-β1 with TβRII-ED. **a** The superposition of crystal structure (*yellow part*) and docked structure (*colored part*). In the docked structure, the α-helix is represented by red color, the β-sheet is represented by *cyan color* and the β-turn is represented by *green color*. The Zrank score is −96.45. **b** The residues of TGF-β1 are present in stick style, and the residues of TβRII-ED are present in ball-stick style. The interactions between TGF-β1 and TβRII-ED involve five TGF-β1 residues (Arg25, His34, Tyr91, Gly93, and Arg94) at the tips of its fingers and four TβRII-ED residues (Asp32, Thr51, Ser52, Ile53 and Asp118)

Table 1 The van Der Waals (E_{vdw}), electrostatic (E_{ele}) and total energy (E_{total}) between some important TβRII-ED residues and TGF-β1 subunit (PDB ID:3KFD) (kcal·mol^{-1})

Residue	Crystal structure of TβRII-ED			Docking structure of TβRII-ED		
	E_{vdw}	E_{ele}	E_{total}	E_{vdw}	E_{ele}	E_{total}
Pro25	−0.13	−2.33	−2.46	−0.01	−2.39	−2.40
Leu27	−4.56	2.68	−1.88	−1.00	−0.88	−1.88
Cys28	−0.24	−2.92	−3.16	−0.01	−3.32	−3.33
Phe30	−4.86	−9.59	−14.45	−0.84	−10.80	−11.64
Asp32	2.12	−123.15	−121.03	3.58	−129.03	−125.45
Val33	−0.06	−2.16	−2.22	−0.05	−1.29	−1.34
Ser46	0.00	−5.21	−5.21	0.00	−5.40	−5.40
Asn47	–	–	–	0.00	−2.16	−2.16
Cys48	−0.11	−14.30	−14.41	−0.15	−4.55	−4.70
Thr51	−3.80	0.43	−3.37	−0.01	−5.31	−5.32
Ser52	−5.41	−11.43	−16.84	−0.74	−9.01	−9.75
Ile53	−1.53	−33.40	−34.93	−1.10	−35.51	−36.61
Glu55	−3.89	−89.59	−93.48	−2.66	−71.57	−74.23
Glu59	−0.11	−52.59	−52.70	−0.08	−56.85	−56.93
Val60	0.00	−6.66	−6.66	0.00	−6.65	−6.65
Val62	−0.01	−1.99	−2.00	−0.34	−1.47	−1.81
Val64	–	–	–	0.00	−2.82	−2.82
Glu75	−0.11	−45.93	−46.04	−0.10	−40.51	−40.61
Thr76	−0.09	−6.73	−6.82	−0.02	−6.44	−6.46
Cys78	−0.29	−2.88	−3.17	−1.36	−1.72	−3.08
Asp80	0.00	−2.50	−2.50	0.00	−2.82	−2.82
Pro84	0.00	−1.24	−1.24	0.00	−2.08	−2.08
Ser95	–	–	–	0.00	−3.16	−3.16
Pro96	0.00	−6.00	−6.00	0.00	−4.34	−4.34
Asp118	−0.93	−79.64	−80.57	−1.06	−94.00	−95.06
Total	−24.01	−497.13	−521.14	−5.95	−504.08	−510.03

Twenty ns MD simulations were also performed for TβRII-ED:nVAP and TβRI-ED:nVAP complex with Amber10 to evaluate the stability of the complexes. The protocol settings were the same as nVAP dynamic process.

Results and discussion

Homology modeling of nVAP

An accurate modeling structure originates from a high level of sequence identity between the target and template sequence. Here, we performed a multiple sequences alignment on the basis of the template protein from different species. In the result of the FASTA search, chain A of 1IBE from horse has a high level of sequence identity and the sequence identity with nVAP is 81 %. Chain A of 1FAW from goose has 62 % identity. Chain A of 3AT5 from turtle has 53 % identity, and a template protein from deer, chain A of 1HDS, has 78 % identity. Besides, some experimental research shows that nVAP is a characteristic polypeptide from *Cervus nippon Temminck* [1]. Therefore, it indicates that nVAP is not separated from cervinus hemoglobin but an independent entity abstracted from velvet antler. All of the above evidence allows for rather straightforward sequence alignment (Fig. 2) and structural modeling. The sequence of nVAP shows that it is abundant in glycine, valine, leucine and lysine, without cysteine. In our study, automated homology model building is performed using a protein structure modeling program Modeler. With this procedure, five initial models are constructed. Finally, the model with the highest score is chosen and used to be the following refinement. This model is refined by MM optimization and MD simulations, and then the final stable structure of nVAP is obtained. The shape of nVAP looks like a letter "V" (Fig. 3). It contains two α-helixes. The angle of two helixes is about 52°. One helix is composed of Asp6 to Gly15. The other is composed of Ala21 to Ala28. The Procheck is used to calculate the percent of backbone θ-φ angles within

the allowed Ramachandran region. The result is that 96.9 % of the θ-φ angles in the nVAP model lie in the core region of the Ramachandran plot (Fig. 4). The final structure is further checked by Profile-3D and the results are presented in Fig. 5. When checked by Profile-3D, the self-compatibility score for this protein is 8.13, which is higher than the low score 6.44. Note that compatibility scores above zero correspond to 'acceptable' side chain environment. From Fig. 5, it is shown that all residues are reasonable. The root mean square deviation (RMSD) of the Cα atoms between the initial model and final model of nVAP is 0.7 Å, which keeps stable after 4.5 ns (Fig. 6a). The above results indicate that the homology model is reliable.

Docking studies

Evaluation of ZDOCK by the docking of TβRII-ED:TGF-β1 complex

In order to evaluate the reliability of the present docking method, we performed the docking of TGF-β1 to TβRII-ED in 3KFD. The docked structure TβRII-ED:TGF-β1 was superimposed with the crystal TβRII-ED:TGF-β1 complex [27] (Fig. 7a). The RMSD of the two structures was 1.061 Å. In order to investigate the interaction between TβRII-ED and TGF-β1, the binding site in TβRII-ED was defined as a subset that contains residues in which any atom is within 10 Å from TGF-β1. Hydrogen bonds play an important role in structure and function of TβRII-ED:TGF-β1 complex. Seven hydrogen bonds are formed in the docked complex of TGF-β1 to TβRII-ED (Fig. 7b, Table 1), which is consistent with the crystal structure [27]. These hydrogen bonds, which enhance the stability of the TβRII-ED:TGF-β1 complex, are presented as follows:

Carboxyl O of TβRII-ED Asp32 … guanidino H of TGF-β1 Arg94,
Hydroxyl O of TβRII-ED Thr51 … imidazole H of TGF-β1 His34,
Amino H of TβRII-ED Ile53 … carbonyl O of TGF-β1 Tyr91,
Carbonyl O of TβRII-ED Ile53 … amino H of TGF-β1 Gly93,
Two carboxyl Os of TβRII-ED Asp118 … two amino Hs of TGF-β1 Arg25

The interaction energy on TβRII-ED and TGF-β1 is shown in Table 1. It gives the interaction energies with total energies lower than −1 kcal·mol^{-1}, including the van der Waals (E_{vdw}), electrostatic (E_{ele}) and total (E_{total}) energies. These interactions determine a stable binding mode for TβRII-ED:TGF-β1 complex (Table 1). Through the residue interaction analysis, Phe30, Asp32, Thr51, Ser52, Ile53 and

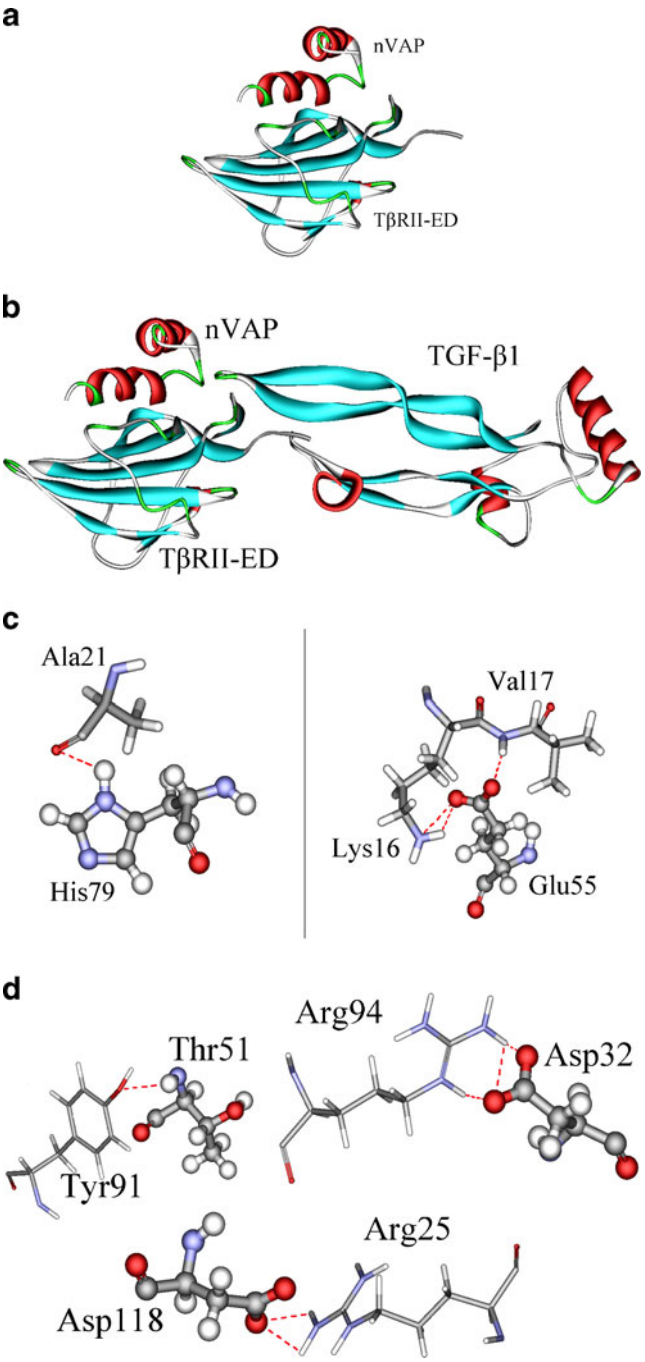

Fig. 8 **a** The docking conformation of nVAP:TβRII-ED complex. **b** The docking conformation of nVAP:TβRII-ED:TGF-β1 ternary complex. There is 10.5° rotation for TGF-β1 around binding site with TβRII-ED complex forward and 30.0° rotation for TGF-β1 abscissa axial direction backward comparing with the former Fig. 7a docking structure. **c** The residues of nVAP are presented in stick style, and TβRII-ED are presented in ball-stick style. nVAP possess the binding site of TβRII-ED for TGF-β1 partially. Lys16, Val17 and Ala21 of nVAP interact with Glu55 and His79 of TβRII-ED in four hydrogen bonds. The Zrank score of nVAP:TβRII-ED complex is −79.489. **d** The residues of TβRII-ED are presented in ball-stick style, and the residues of TGF-β1 are presented in slender-stick style. Comparing with the former docking of TGF-β1 and TβRII-ED, the hydrogen bonds attenuate apparently. The Zrank score of TGF-β1 and nVAP:TβRII-ED complex is −93.911

Table 2 The van Der Waals (E_{vdw}), electrostatic (E_{ele}) and total energy (E_{total}) between some important TβRII-ED residues and nVAP or TGF-β1 subunit in TGF-β1:TβRII-ED: nVAP complex, (kcal·mol^{-1})

TβRII-ED:nVAP complex				TβRII-ED:TGF-β1 complex			
Residue	E_{vdw}	E_{ele}	E_{total}	Residue	E_{vdw}	E_{ele}	E_{total}
Leu27	−0.01	−2.85	−2.86	Val22	−0.60	−4.10	−4.70
Phe30	−0.05	−6.16	−6.21	Pro25	−2.84	−12.22	−15.06
Arg34	0.00	−1.91	−1.91	Lys29	−0.28	−10.59	−10.87
Ser52	−0.49	−3.34	−3.83	Phe30	−3.58	−2.92	−6.50
Ile53	−0.28	−2.86	−3.14	Cys31	−0.43	−5.79	−6.22
Glu55	−0.89	−7.91	−8.80	Val33	−0.06	−3.23	−3.29
Cys61	−0.05	−2.28	−2.33	Ser46	0.00	−5.39	−5.39
Val62	−0.28	−1.11	−1.39	Cys48	−0.05	−3.83	−3.88
Thr76	−0.08	−4.16	−4.24	Cys54	−0.92	−5.83	−6.75
His79	−0.36	−9.84	−10.20	Glu55	−2.29	−74.90	−77.19
Leu83	−1.64	−25.73	−27.37	Pro57	−0.16	−9.56	−9.72
Tyr85	−2.01	−11.18	−13.19	Glu59	−0.08	−42.75	−42.83
Phe88	−1.19	−11.63	−12.82	Val60	−0.01	−1.09	−1.10
Glu91	−0.01	−1.77	−1.78	Val62	0.00	−3.14	−3.14
Lys104	0.00	−3.47	−3.47	Glu75	−0.06	−33.31	−33.37
Glu108	0.00	−8.77	−8.77	Cys78	−0.15	−5.24	−5.39
				Tyr85	−0.03	−2.90	−2.93
				Ala93	0.00	−8.17	−8.17
				Ala94	0.00	−1.65	−1.65
				Ser95	0.00	−5.08	−5.08
				Pro96	0.00	−3.41	−3.41
				Ser116	−0.07	−20.98	−21.05
				Asp118	91.89	−169.03	−77.14
				Glu119	−0.94	−38.53	−39.47
				Asp122	−0.01	−8.69	−8.70
Total	−7.34	−104.97	−112.31		79.33	−482.33	−403.00

Asp118 are important anchoring residues for TGF-β1 [27] (Table 1). The E_{total} of crystal structure is −521.14 kcal·mol^{-1}. The E_{total} is −510.03 kcal·mol^{-1} and total anchoring energy is −283.8 kcal·mol^{-1}. Comparing with TβRII-ED:TGF-β1 crystal structure, the docking results and energy indicate that it is reliable for further simulations.

Interactions of nVAP and TβRII-ED:TGF-β1 complex

In order to investigate the interaction between nVAP and TβRII-ED:TGF-β1 complex, the binding pocket is defined as a subset that contains residues in which any atoms are within 10.0 Å from TβRII-ED. The active site is obtained using Discovery Studio 2.5/ZDOCK module [24], and the locations of the site in the 3D structure of TβRII-ED:TGF-β1 complex are shown in Fig. 8b. The binding site is composed of 16 residues (Table 2). Based on our theoretically predicted results, this site is chosen as the more favorable binding site to dock the nVAP in this study.

The conformational characteristics of TβRII-ED:nVAP complex, TβRII-ED and nVAP were investigated by using MD simulation method at 300 K with explicit water (Fig. 6b). After 20 ns molecular dynamics simulation, the average RMSD value of TβRII-ED:nVAP complex is 2.88 Å (standard deviation: 0.27 Å). For TβRII-ED and nVAP, the average RMSD values are 2.44 Å (0.14 Å) and 2.68 Å (0.29 Å), respectively, indicating the docked complex structures are stable [28]. The interaction energy on nVAP:TβRII-ED complex is −134.13 kcal·mol^{-1}. To determine the interaction energies between the residues of nVAP and TβRII-ED, significant binding-site residues were identified by the total interaction energy in TβRII-ED:nVAP complex. This identification can clearly show the relative significance for every

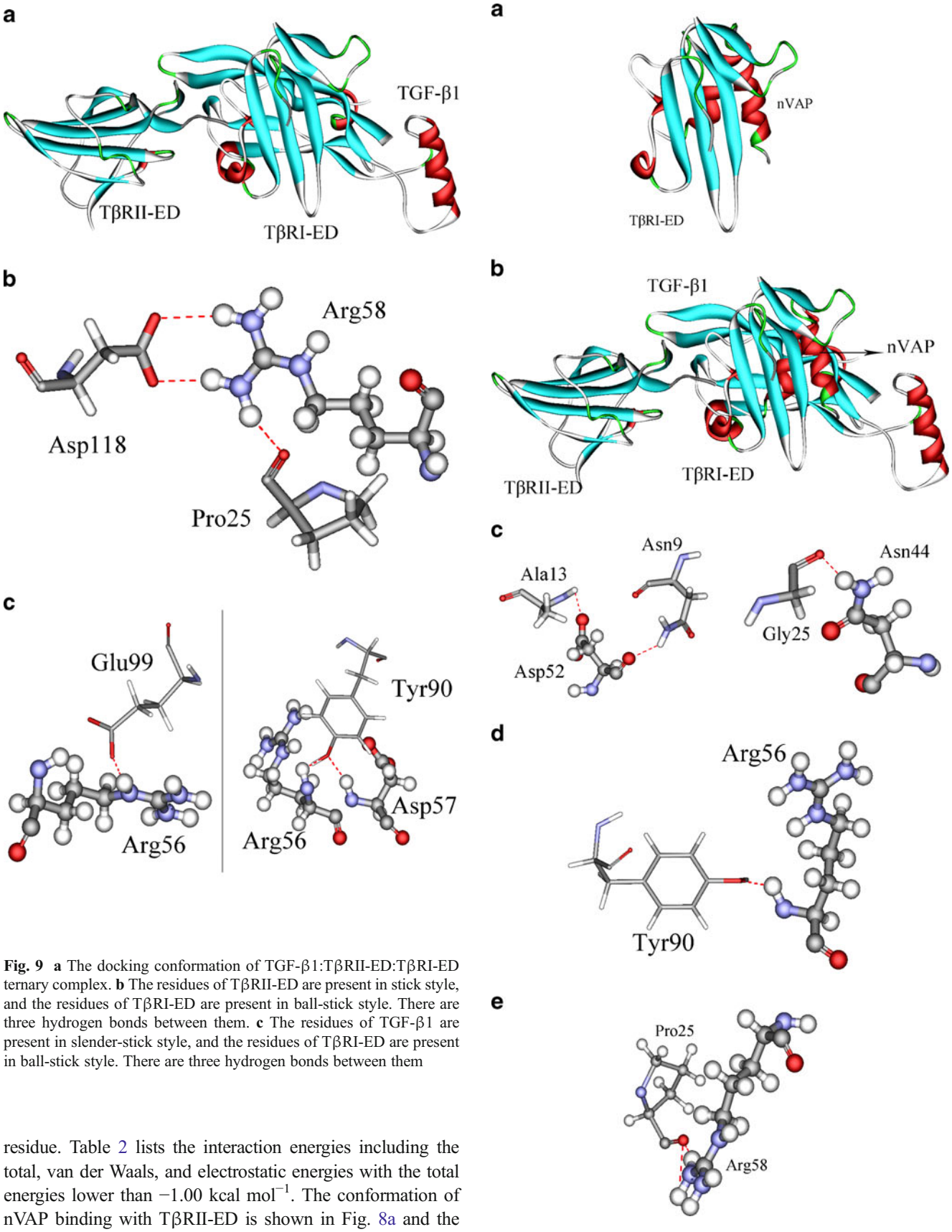

Fig. 9 **a** The docking conformation of TGF-β1:TβRII-ED:TβRI-ED ternary complex. **b** The residues of TβRII-ED are present in stick style, and the residues of TβRI-ED are present in ball-stick style. There are three hydrogen bonds between them. **c** The residues of TGF-β1 are present in slender-stick style, and the residues of TβRI-ED are present in ball-stick style. There are three hydrogen bonds between them

residue. Table 2 lists the interaction energies including the total, van der Waals, and electrostatic energies with the total energies lower than −1.00 kcal mol^{-1}. The conformation of nVAP binding with TβRII-ED is shown in Fig. 8a and the hydrogen bonds in the complex are shown in Fig. 8c. nVAP forms the interaction with TβRII-ED beside the TGF-β1

◀ **Fig. 10** **a** The docking result between nVAP and TβRI-ED. **b** The recruitment of nVAP:TβRI-ED complex to TGF-β1:TβRII-ED. **c** The residues of nVAP are present in stick style, and the residues of TβRI-ED are present in ball-stick style. There are three hydrogen bonds between nVAP and TβRI-ED. **d** The residues of TGF-β1 are presented in slender-stick style, and the residues of TβRI-ED are presented in ball-stick style. With hydrogen bonds participating in recruitment of nVAP:TβRI-ED, the interacting mode of TβRI-ED is also altered significantly rather than low-affinity with TGF-β1:TβRII-ED complex. **e** The residues of TβRII-ED are present in tenuis ball-stick style, and the residues of TβRI-ED are present in ball-stick style

binding site (Fig. 8b). It indicates that the inhibiting mechanism of nVAP is noncompetitive inhibition which interacts with TβRII-ED. Phe30, Glu55, His79, Leu83, Tyr85, and Phe88 are the anchoring residues of nVAP:TβRII-ED complex and have main contribution to the complex interaction (Table 2). In the docked conformation of nVAP:TβRII-ED:TGF-β1 ternary complex (Fig. 8b, Table 2), the anchoring residues of TβRII-ED are as follows: Pro25, Phe30, Glu55, Asp118, Glu119. Compared with the former 3KFD docked structure (Fig. 7a), the E_{total} and total residue anchoring energy of TβRII-ED is increased to −403.01 and −215.4 kcal·mol^{-1}, respectively. In the docked structure, Phe30 and Glu55 of TβRII-ED have the main contribution to the stability of nVAP:TβRII-ED complex and TGF-β1:TβRII-ED complex. Around Phe30 of TβRII-ED, there are Cys31 and Cys78 of TβRII-ED, and Val17, Gly18 of nVAP forming a hydrophobic area (Table 2). Meanwhile, Glu55 of TβRII-ED and Lys16 of nVAP form strong salt-bridge interaction (Fig. 8c). Apart from this, the interactions of the rest residues change a lot after nVAP docking with TβRII-ED, which have minor effect on TGF-β1 binding with TβRII-ED. The role of TβRII-ED is to anchor the TGF-β1 and TβRI-ED to a proper conformation [29]. The interaction energy on TGF-β1:TβRII-ED complex is decreased after nVAP binding with TβRII-ED, which would have effect on TGF-β1 signaling though the downstream functional domains of TβRI-ED.

Identification of binding region in TβRI-ED:TGF-β1 complex and TβRI-ED:TβRII-ED complex

TβRI-ED is from TGF-β3:TβRII-ED:TβRI-ED complex (PDB code: 2PJY chain C), which shares common structure in TGF-β complex family signaling pathways [30]. TGF-β1 and TβRII-ED were obtained from PDB ID: 3KFD chain A and E. First, we docked TβRII-ED and TGF-β1. Then TβRI-ED was docked with TβRII-ED:TGF-β1 complex to form the ternary complex (Figs. 7a, 9a). The interaction energy on TβRI-ED is shown in Table 3. The E_{total} of TβRI-ED:TβRII-ED complex is −179.54 kcal·mol^{-1}, and E_{total} of TβRI-ED:TGF-β1 complex is −68.61 kcal·mol^{-1}.

Table 3 The van Der Waals (E_{vdw}), electrostatic (E_{ele}) and total energy (E_{total}) between some important TβRI-ED residues and TβRII-ED or TGF-β1 subunit in TGF-β1: TβRI-ED: TβRII-ED ternary complex (kcal·mol^{-1})

TβRI-ED:TGF-β1 complex				TβRI-ED:TβRII-ED complex			
Residue	E_{vdw}	E_{ele}	E_{total}	Residue	E_{vdw}	E_{ele}	E_{total}
Gly28	−0.01	−6.90	−6.91	Leu29	−0.17	−4.67	−4.84
Leu29	−0.01	−5.81	−5.82	Cys30	−0.04	−8.43	−8.47
Ile51	5.93	−8.46	−2.53	Glu36	0.00	−5.40	−5.40
Leu53	−0.97	−1.08	−2.05	Ile48	−0.01	−1.43	−1.44
Pro55	3.97	−9.60	−5.63	Leu53	−0.04	−1.47	−1.51
Arg56	0.44	−2.48	−2.04	Arg58	83.00	−134.82	−51.82
Asp57	8.00	−19.09	−11.09	Phe60	−0.11	−4.55	−4.66
Pro59	−0.53	−4.91	−5.44	Ala63	−0.51	−6.16	−6.67
Phe60	−3.00	−2.46	−5.46	Ser65	−0.03	−4.08	−4.11
Val61	−0.14	−8.19	−8.33	Lys67	−1.49	−58.41	−59.90
Pro64	0.00	−3.37	−3.37	Thr68	−0.01	−2.50	−2.51
Ser66	0.00	−5.10	−5.10	Thr72	0.00	−1.44	−1.44
Thr68	−0.01	−4.83	−4.84	Thr74	−0.36	−5.75	−6.11
				Asn78	−0.08	−9.56	−9.64
				Cys82	−0.02	−3.03	−3.05
				Lys84	0.00	−4.57	−4.57
				Glu86	0.00	−3.40	−3.40
Total	13.67	−82.28	−68.61		80.13	−259.67	−179.54

There are three hydrogen bonds between TβRI-ED and TβRII-ED (Fig. 9b):

Two guanidino Hs of TβRI-ED Arg58 … two carboxyl Os of TβRII-ED Asp118,
Guanidino H of TβRI-ED Arg58 … carbonyl O of TβRII-ED Pro25,
Three hydrogen bonds also interact with TβRI-ED and TGF-β1 (Fig. 9c):
Guanidino H of TβRI-ED Arg56 … carbonyl O of TGF-β1 Glu99,
Peptide bond H of TβRI-ED Arg56 … phenolic O of Tyr90,
Peptide bond H of TβRI-ED Asp57 … phenolic O of Tyr90.

There is a "pre-helix extension" including Pro55, Arg56, Asp57, Arg58, Pro59, which are highly conserved flanking amino acids, forming a sharply curved, finger-like projection [29]. It contributes recruitment to both TβRII-ED and TGF-β1. Arg58 of TβRI-ED has −134.82 kcal·mol^{-1} of E_{ele} and −51.82 kcal·mol^{-1} of E_{total} (Table 3). Asp118 of TβRII-ED (Fig. 7b, Table 1) plays the important role in binding with TβRII-ED and recruiting TβRI-ED by electrostatic force. The total energy of Pro55, Arg56, Asp57, Pro59, is −24.21 kcal·mol^{-1} recruited into TGF-β1 with low affinity.

Interactions of nVAP and TβRI-ED:TβRII-ED:TGF-β1 complex

The conformational characteristics of TβRI-ED:nVAP complex, TβRI-ED and nVAP were investigated by using MD simulation method at 300 K with explicit water. The TGF-β1 and TβRII-ED in the quaternary complex were obtained from the TGF-β1:TβRII-ED docking structure. The distributions of RMSD of TβRI-ED:nVAP, TβRI-ED, and nVAP with respect to their initial structures are displayed in Fig. 6c. During 20 ns simulations, the average RMSD values for all

Table 4 The van Der Waals (E_{vdw}), electrostatic (E_{ele}) and total energy (E_{total}) between some important TβRI-ED residues and nVAP, TβRII-ED or TGF-β1 subunit in TGF-β1:TβRI-ED: TβRII-ED: nVAP quaternary complex (kcal·mol^{-1})

TβRI-ED:nVAP complex				TβRI-ED:TGF-β1 complex				TβRI-ED:TβRII-ED complex			
Residue	E_{vdw}	E_{ele}	E_{total}	Residue	E_{vdw}	E_{ele}	E_{total}	Residue	E_{vdw}	E_{ele}	E_{total}
Leu10	−0.13	−6.52	−6.65	Gly28	0.00	−4.21	−4.21	Leu29	−0.12	−4.35	−4.47
Gln11	−0.07	−1.41	−1.48	Leu29	0.00	−4.30	−4.30	Cys30	−0.03	−6.54	−6.57
Phe13	−0.18	−3.74	−3.92	Ala49	−0.02	−0.99	−1.01	Val34	−0.01	−5.88	−5.89
His15	−1.79	−4.95	−6.74	Glu50	−0.38	−11.02	−11.40	Glu36	0.00	−14.45	−14.45
Thr23	−0.25	−0.89	−1.14	Pro59	−0.31	−7.24	−7.55	Ile54	−0.10	−2.38	−2.48
Thr26	6.86	−16.73	−9.87	Val61	−0.07	−7.27	−7.34	Pro55	−0.68	−2.63	−3.31
Asp27	−1.03	−110.51	−111.54	Ala63	−0.01	−1.79	−1.80	Ala63	−1.86	−5.38	−7.24
Leu29	−0.17	−2.50	−2.67	Ser66	0.00	−5.42	−5.42	Thr73	−0.21	−3.93	−4.14
Cys30	−0.13	−12.02	−12.15	Thr68	−0.01	−3.16	−3.17	Thr74	−0.97	−8.27	−9.24
Phe31	−1.46	−8.63	−10.09	Gly69	0.00	−1.43	−1.43	Cys82	−0.01	−3.50	−3.51
Val34	−0.17	−8.24	−8.41					Lys84	0.00	−4.21	−4.21
Lys40	−0.37	−77.27	−77.64								
Val41	−0.07	−4.12	−4.19								
Glu50	−0.77	−35.80	−36.57								
Leu53	−0.53	−10.70	−11.23								
Pro55	−0.20	−0.94	−1.14								
Cys62	−0.26	−0.97	−1.23								
Ser65	−0.02	−2.74	−2.76								
Thr68	−0.82	−12.49	−13.31								
Gly69	−0.18	−8.96	−9.14								
Val71	−0.14	−3.84	−3.98								
Thr74	−0.19	−5.38	−5.57								
Total	−2.07	−339.35	−341.42		−0.80	−46.83	−47.63		−3.99	−61.52	−65.51

proteins stay at 4.34 Å (standard deviation: 0.24 Å), 4.24 Å (0.26 Å), and 4.33 Å (0.31 Å) for TβRI-ED:nVAP, TβRI-ED, and nVAP, respectively. Although the average RMSD of TβRI-ED:nVAP complex is high up to 4.14 Å, TβRI-ED and nVAP subunits have close RMSD variation compared with the complex. The standard deviations of the three reveal the plots fluctuate mildly along 20 ns MD simulations. The data above show that TβRI-ED has strong interaction with nVAP indicating the docked structure of the complex is stable [28]. Comparing with the RMSD trajectory of nVAP:TβRII-ED, nVAP:TβRI-ED complex is more compatible along the MD simulation (Fig. 6b and c). The interaction energy on nVAP:TβRI-ED complex is −293.84 kcal·mol^{-1}. From the compared results of conformations and interaction energies, nVAP shows higher affinity binding with TβRI-ED rather than TβRII-ED (134.13 kcal·mol^{-1}). The docked site of TβRI-ED is consistent with peptide:TβR binding result [31, 32]. The docked conformation shows that the inhibiting mechanism of nVAP is competitive inhibition which interacts with TβRI-ED. The docked results show that nVAP generates major inhibitory action on TβRI-ED, and minor inhibitory action on TβRII-ED, which is common to most TβR inhibitors [33]. When the TβRI-ED is recruited to TβRII-ED:TGF-β1 complex, nVAP molecule occupies the interface of pre-helix extension which plays a central role in TGF-β and TβRII-ED interaction (Fig. 10a and b) [29]. In TGF-β1:TβRII-ED:TβRI-ED:nVAP quaternary structure, the interaction of TβRI-ED:TGF-β1 and TβRI-ED:TβRII-ED complexes are changed significantly by the insertion of nVAP on TβRI-ED (Fig.10c, d and e). The total energy of TβRI-ED:TGF-β1 interface residues increases from −68.61 kcal·mol^{-1} to −47.65 kcal·mol^{-1}. The total energy of TβRI-ED:TβRII-ED interface residues increases from −179.54 kcal·mol^{-1} to −65.50 kcal·mol^{-1} (Tables 3, 4). The total energy of "pre-helix extension" recruited to TGF-β1 and TβRII-ED increases from −76.03 kcal·mol^{-1} to −10.86 kcal·mol^{-1}. TβRI-ED and TβRII-ED do not conform properly with the binding of nVAP respectively. Thus, intracellular domain of TβRI can not be correctly phosphorylated without the low-affinity of TβRII-ED to TβRI-ED, causing the downstream intracellular pathway to be blocked. Once the pathway is intercepted, the TGF-β1 signaling can not be transmitted intracellularly.

TGF-β1 can obstruct cell cycle in G0 period, which induces the G0 cells such as hepatic cells to apoptosis [34]. Otherwise, TGF-β1 comes from Kupffer cell and activates the hepatic stellate cell (HSC). TGF-β1 is also expressed in HSC secondarily, further promotes HSC to transform into myofibroblast where the ECM is generated and secreted [35–37]. nVAP facilitates proliferation of hepatic cells in cell culture experiment [1]. Our studies indicate the mechanism of nVAP to prevent the progress of hepatic fibrosis and provide support for further studies in molecular levels.

Conclusions

The 3D structure of natural velvet antler polypeptide (nVAP) has not been known before. In this investigation, the 3D structure of nVAP was built by homology modeling, which was based on the known crystal structures of hemoglobin (PDB code: 1HDS, 1IBE, 1FAW, 3AT5), and then energy minimization and molecular dynamics were used to refine the structure. With this model, a protein-protein docking study was performed by ZDOCK module. The docking results of TGF-β1:TβRII-ED:TβRI-ED ternary complex indicate that Phe30, Asp32, Thr51, Ser52, Ile53, Asp118 of TβRII-ED could stabilize the position and orientation in the active site of TGF-β1. "Pre-helix extension" of TβRI-ED including Pro55, Arg56, Asp57, Arg58, Pro59, is the key domain recruited to both TβRII-ED and TGF-β1. After docked with TβRII-ED (−112.31 kcal·mol^{-1}) and TβRI-ED (−341.45 kcal·mol^{-1}), nVAP changes the binding mode of TGF-β1 complex. The results show that nVAP has higher affinity with TβRI-ED and lower affinity with TβRII-ED. The interaction between TβRII-ED and TGF-β1 increases from −510.03 kcal·mol^{-1} to −403.01 kcal·mol^{-1}, TβRI-ED and TGF-β1 augments from −68.61 kcal·mol^{-1} to −47.65 kcal·mol^{-1}, TβRI-ED and TβRII-ED increases from −179.54 kcal·mol^{-1} to −65.50 kcal·mol^{-1}. With the binding of nVAP, the interaction energy between TGF-β1 and TβR-EDs decreased and the H-bond number also reduced, which shows that nVAP might effect TGF-β1 signaling pathway.

Acknowledgments This work is supported by Natural Science Foundation of China, Specialized Research Fund for the Doctoral Program of Higher Education, and Specialized Fund for the Basic Research of Jilin University and 2011 Postgraduate Innovative Research Project of Jilin University (Grant Nos. 21273095, 20903045, 21203072, 20070183046, 201003044 and 20111067).

References

1. Guan SW, Duan LX, Li YY, Wang BX, Zhou QL (2006) A novel polypeptide from Cervus nippon Temminck proliferation of epidermal cells and NIH3T3 cell line. Acta Biochim Pol 53:395–397
2. Plum J, De Smedt M, Leclercq G, Vandekerckhove B (1995) Influence of TGF-beta on murine thymocyte development in fetal thymus organ culture. J Immunol 154:5789–5798
3. Wahl SM, Swisher J, McCartney-Francis N, Chen WJ (2004) TGF-beta: the perpetrator of immune suppression by regulatory T cells and suicidal T cells. J Leukoc Biol 76:15–24
4. Wu DT, Bitzer M, Ju W, Mundel P, Bottinger EP (2005) TGFβ concentration specifies differential signaling profiles of growth arrest/differentiation and apoptosis in podocytes. J Am Soc Nephrol 16:3211–3221
5. Border WA, Noble NA (1994) Transforming growth factor beta in tissue fibrosis. N Engl J Med 331:1286–1292

6. Derynck R, Zhang Y, Feng XH (1998) Smads: transcriptional activators of TGF-beta responses. Cell 95:737–740
7. Yingling JM, Blanchard KL, Sawyer JS (2004) Development of TGF beta signalling inhibitors for cancer therapy. Nat Rev Drug Discov 3:1011–1022
8. Karlsson G, Liu Y, Larsson J, Goumans MJ, Lee JS, Thorgeirsson SS, Ringner M, Karlsson S (2005) Gene expression profiling demonstrates that TGF-beta 1 signals exclusively through receptor complexes involving Alk5 and identifies targets of TGF-beta signaling. Physiol Genomics 21:396–403
9. Laping NJ, Everitt JI, Frazier KS, Burgert M, Portis MJ, Cadacio C, Gold LI, Walker CL (2007) Tumor-specific efficacy of transforming growth factor-beta RI inhibition in Eker rats. Clin. Cancer Res 13:3087–3099
10. Laping NJ, Huet S (2006) In: Dijke P, Heldin CH (eds) TGFβ receptor kinase inhibitors for treatment of fibrosis smad signal transduction, vol 5. Springer, Netherlands, pp 443–459
11. Suzuki E, Kim S, Cheung HK, Corbley MJ, Zhang X, Sun L, Shan F, Singh J, Lee WC, Albelda SM, Ling LE (2007) A novel small-molecule inhibitor of transforming growth factor beta type I receptor kinase (SM16) inhibits murine mesothelioma tumor growth in vivo and prevents tumor recurrence after surgical resection. Cancer Res 67:2351–2359
12. Fu K, Corbley MJ, Sun L, Friedman JE, Shan F, Papadatos JL, Costa D, Lutterodt F, Sweigard H, Bowes S, Choi M, Boriack Sjodin PA, Arduini RM, Sun D, Newman MN, Zhang X, Mead JN, Chuaqui CE, Cheung HK, Zhang X, Cornebise M, Carter MB, Josiah S, Singh J, Lee WC, Gill A, Ling LE (2008) SM16, an orally active TGF-beta type I receptor inhibitor prevents myofibroblast induction and vascular fibrosis in the rat carotid injury model. Arterioscl Throm Vas 28:665–671
13. Wrana JL, Attisano L, Carcamo J, Zentella A, Doody J, Laiho M, Wang XF, Massague J (1992) TGF beta signals through a heteromeric protein kinase receptor complex. Cell 71:1003–1014
14. Wrana JL, Attisano L, Wieser R, Ventura F, Massague J (1994) Mechanism of activation of the TGF-[beta] receptor. Nature 370:341–347
15. Greenwald J, Fischer WH, Vale WW, Choe S (1999) Three-finger toxin fold for the extracellular ligand-binding domain of the type II activin receptor serine kinase. Nat Struct Biol 6:18–22
16. Crescenzo GD, Grothe S, Lortie R, Debanne MT, O'Connor-McCourt M (2000) Real-time kinetic studies on the interaction of transforming growth factor alpha with the epidermal growth factor receptor extracellular domain reveal a conformational change model. Biochem 39:9466–9476
17. Altschul SF, Madden TL, Schfer AA, Zhang JH, Zhang Z, Miller W, Lipman DJ (1997) Gapped BLAST and PSI-BLAST: a new generation of protein database search programs. Nucleic Acids Res 25:3389–3402
18. Accelrys Software Inc (2007) Discovery studio user guide. Accelrys Software Inc, San Diego
19. Case DA, Cheatham TE III, Darden T, Gohlke H, Luo R, Merz KM Jr, Onufriev A, Simmerling C, Wang B, Woods RJ (2005) The Amber biomolecular simulation programs. J Comput Chem 26:1668–1688
20. Ode H, Matsuyama S, Hata M, Hoshino T, Kakizawa J, Sugiura W (2007) Mechanism of drug resistance due to N88S in CRF01_AE HIV-1 protease, analyzed by molecular dynamics simulations. J Med Chem 50:1768–1777
21. Jorgensen WL, Chandraskhar J, Madura J, Impey RW, Klein ML (1983) Comparison of simple potential functions for simulating liquid water. J Chem Phys 79:926–935
22. Biosym/MSI (2000) Insight II profile 3D user guide. Biosym/MSI, San Diego
23. Laskowski R, Macarthur MW, Moss DS, Thornton JM (1993) PROCHECK: a program to check the stereochemical quality of protein structures. J Appl Crystallogr 26:283–291
24. Wiehe K, Pierce B, Mintseris J, Tong WW, Anderson R, Chen R, Weng Z (2005) ZDOCK and RDOCK performance in CAPRI rounds 3, 4, and 5. Proteins 60:207–213
25. Grosdidier A, Zoete V, Michielin O (2011) Fast docking using the CHARMM force field with EADock. DSS J Comput Chem 32:2149–2159
26. Khan AU, Baig MH, Wadhwa G (2011) Molecular docking analysis of new generation cephalosporins interactions with recently known SHV-variants. Bioinformation 5:331–335
27. Radaev S, Zou ZC, Huang T, Lafer EM, Hinck AP, Sun PD (2010) Ternary complex of transforming growth factor-β1 reveals isoform-specific ligand recognition and receptor recruitment in the superfamily. J Biol Chem 285:14806–14814
28. Perez A, Luque FJ, Orozco M (2007) Dynamics of B-DNA on the microsecond time scale. J Am Chem Soc 129:14739–14745
29. Groppe J, Hinck CS, Payman ST, Zubieta C, Schuermann JP, Taylor AB, Schwarz PM, Wrana JL, Hinck AP (2008) Cooperative assembly of TGF-β superfamily signaling complexes is mediated by two disparate mechanisms and distinct modes of receptor binding. Mol Cell 29:157–168
30. Mittl PRE, Priestle JP, Cox DA, McMaster G, Cerletti N, Grutter MG (1996) The crystal structure of TGF-beta 3 and comparison to TGF-beta 2: implications. Protein Sci 5(7):1261–1271
31. Moreira IS, Fernandes PA, Ramos MJ (2007) Hot spots—A review of the protein–protein interface determinant amino–acid residues. Proteins 68:803–812
32. Li L, Orner BP, Huang T, Hinck AP, Kiessling LL (2010) Peptide ligands that use a novel binding site to target both TGF-β receptors. Mol Biosyst 6:2392–2402
33. Ren JX, Li LL, Zou J, Yang L, Yang JL, Yang SY (2009) Pharmacophore modeling and virtual screening for the discovery of new transforming growth factor-[beta] type I receptor (ALK5) inhibitors. Eur J Med Chem 44:4259–4265
34. Hu MG, Hu GF, Kim Y, Tsuji T, McBride J, Hinds P, Wong DTW (2004) Role of p12CDK2-AP1 in transforming growth factor-β1-mediated growth suppression. Cancer Res 15:490–499
35. Gressner AM, Weiskirchen R, Breitkopf K, Dooley S (2002) Roles of TGF-beta in hepatic fibrosis. Front Biosci 7:793–807
36. Dooley S, Delvoux B, Lahme B, Mangasser-Stephan K, Gressner AM (2000) Modulation of transforming growth factorβ response and signaling during transdifferentiation of rat hepatic stellate cells to myofibroblasts. Hepatology 31:1094–1106
37. Gressner AM, Gao CF (1995) A cascade-mechanism of fat storing cell activation forms the basis of the fibrogenic reaction of the liver. Verh Dtsch Ges Pathol 79:1–14